Volume 23 (2004), number 4 pp. 783–797 COMPUTER GRAPHICS *forum*

Para-Graph: Graph-Based Parameterization of Triangle Meshes with Arbitrary Genus

Giuseppe Patanè, Michela Spagnuolo and Bianca Falcidieno

Istituto di Matematica Applicata e Tecnologie Informatiche, Consiglio Nazionale delle Ricerche, Genova, Italy

Abstract

This paper describes a novel approach to the parameterization of triangle meshes representing 2-manifolds with an arbitrary genus. A topology-based decomposition of the shape is computed and used to segment the shape into primitives, which define a chart decomposition of the mesh. Then, each chart is parameterized using an extension of the barycentric coordinates method. The charts are all 0-genus and can be of three types only, depending on the number of boundary components. The chart decomposition and the parameterization are used to define a shape graph where each node represents one primitive and the arcs code the adjacency relationships between the primitives. Conical and cylindrical primitives are coded together with their skeletal lines that are computed from and aligned with their parameterization. The application of the parameterization approach to remeshing guarantees that extraordinary vertices are localized only where two patches share a boundary and they are not scattered on the whole surface.

Keywords: Parameterization, Reeb graph, remeshing

ACM CCS: I.3.5 Computer Graphics: Curve, surface, solid and object representations

1. Introduction

The parameterization of 2D manifold triangle meshes has been largely analyzed in *Computer Graphics* due both to its theoretical importance for surface classification and impact on applications such as texture mapping, compression and animation. While the parameterization of manifolds homeomorphic to a disk is well understood, the case of surfaces with an arbitrary genus is still a very challenging research topic. This problem is usually approached in two different ways: either the surface is decomposed into a family of disk-like patches (i.e. *local parameterization*, or atlas generation), or a cut is defined on the manifold which is successively unfolded onto a unique planar domain (i.e. *global parameterization*).

Our goal is to devise an atlas generation method for 2-manifold triangle meshes of arbitrary genus, which produces a *canonical* decomposition of the shape, a *minimal* number of charts, a *flexible* decomposition schema able to capture the most interesting shape features and a coding of the parameterization which is *useful* for applications such as editing or deformation.

The crux of the proposed method is the exploitation of the information about both the surface topology for optimizing its decomposition and cutting, and the surface geometry for minimizing the parameterization distortion. The use of topological information provides evident benefits in all subsequent stages of the parameterization and its applications. The proposed approach is applied to remeshing, and produces remeshed shapes whose extraordinary vertices (i.e. with valence different than six) are localized on *smooth boundaries* where adjacent patches join, and they are not scattered on the surface as in previous work.

1.1. Related Work

First of all, for a complete survey on the parameterization of surfaces with genus zero, we refer to the following papers

© The Eurographics Association and Blackwell Publishing Ltd 2004. Published by Blackwell Publishing, 9600 Garsington Road, Oxford OX4 2DQ, UK and 350 Main Street, Malden, MA 02148, USA.

Submitted July 2004
Revised October 2004
Accepted November 2004

[1–3], which contain an extensive discussion on the basic principles and methods of parameterization. Here, we briefly review the achievements in the field which are more relevant to the work presented in the paper.

Local parameterization methods build a segmentation of a mesh into patches homeomorphic to a disk, and then map each of them into the plane by a local convex-combination map. The properties of the segmentation usually depend on the application of the parameterization: for example, for remeshing or morphing purposes, triangle-shaped or quadrilateral-shaped patches are often used to build the base mesh, as they well support subdivision schemes and spline-based representations [4–6]. The main problems to be solved are the smoothness of the mapping across the patch boundaries, the control over the shape and the number of patches, which, for complex shapes, may produce a large number of small charts with simple borders.

The segmentation of a surface M into a family of disk-like regions uses algorithms for mesh decimation [7], e.g. vertex-removal or half-edge-collapse, where the simplified triangular mesh $M_S \subseteq M$ approximates the shape of M, sharing the same genus and provides a correspondence between the points of M and M_S. The number of patches is equal to the number of triangles in M_S, and the simplification is guided by a set of criteria and runs until the coarse mesh is as simple as possible without violating quality measures, which aim to reduce the distortion of the embedding.

The least-squares conformal map proposed in [8] attempts to align patch boundaries with lines of significant curvature over the shape and produces patches with arbitrarily shaped boundaries. Each patch is then parameterized using a quasi-conformal parameterization method, based on the minimization of angle deformations. The approach is robust and can parameterize large charts with complex borders.

In general, an oversegmentation can create distortions along the boundaries of adjacent regions which affect the texture mapping and remeshing results, in spite of local adjustments (e.g. smoothing, re-sampling, constrained boundaries).

The decomposition of the input manifold into a set of arbitrarily shaped patches enables to remesh each chart with a regular subdivision, which cannot be extended to the entire surface due to the induced irregular covering of M; therefore, they achieve only a *semi-regular* remeshing.

Alternatively, an arbitrary surface can be unfolded into a single planar domain, by cutting the surface along a connected path [9]. Using a single patch allows to apply *regular* remeshing and to achieve high compression rates; however, it can create parameterizations with greater distortion and a less uniform sampling with respect to the use of multiple local charts. This phenomenon is mainly due to the difficulty of finding a good cut and of controlling its alignment with sharp features (e.g. high-curvature lines); furthermore, the construction of the cut can create complicated and noisy line networks for unfolding surfaces of high genus.

The computation of a global conformal parameterization of a surface with an arbitrary genus without segmentation has been studied in [10]; the method exploits simplicial homology to slice and open the input mesh which is successively mapped onto the plane. Specialized parameterization of 0-genus surfaces onto a spherical domain are discussed in [11,12].

Existing methods are mainly driven by considerations concerning texture mapping and compression as primary application of the parameterization results. Therefore, the patches are generally not related to features of the surface, and the number of generated patches is mainly driven by error or distortion metrics. In this paper, we present a novel approach in which the parameterization process is guided by the shape of the triangle mesh, by its topological properties, and by the aim of building a centerline skeleton, aligned with the parameterization and which can be used for animation and deformation in a straightforward manner.

1.2. Overview and Contributions

Our approach builds on the shape decomposition method defined in [13,14], which uses the concept of quotient space introduced by Reeb [15,16] to classify manifolds under the action of a real smooth mapping function f. The mapping function induces a segmentation of the manifold into cells, or primitives, related to the critical points of the function. Each cell is 0-genus and only three types of patches are possible, according to the number of their boundary components: *conical primitives* have one boundary, *cylinders* have two and *bodies* have three or more boundary components. Moreover, the connectivity of the segmentation is very simple, because the cells can be adjacent only by a whole boundary component, therefore preventing the creation of corner vertices. The decomposition is canonical in the sense that the properties of the cells and their adjacency are independent of the choice of f. The Reeb quotient space induces a segmentation of the manifold into a family of charts which is minimal with respect to the number of critical points of the mapping function and whose mathematical counterpart is the classification theorem for compact surfaces [16,17].

Chosen any arbitrary function f, the first step of our method is to build the decomposition of the manifold triangle mesh M and to store it in a *shape graph* S_M, whose nodes are the primitives and whose arcs code their adjacency. The method used to build the decomposition is fully described in [13,14] and it will be briefly summarized in the next section.

The second step concerns the parameterization of each cell and is the core of our contribution. Conical primitives are parameterized using the Tutte's method [2,3], while an

© The Eurographics Association and Blackwell Publishing Ltd 2004

extension of this method is presented for cylindrical primitives and a novel iterative cutting procedure is introduced for body primitives. The produced cuts are well shaped and stable with respect to the quality of the input patch in terms of tiny triangles and irregular sampling.

Finally, using the parameterized S_M, a centerline skeleton aligned with the parameterization is built, which is very well-suited for deformation and editing.

The decomposition method as well as the parameterization of the primitives is fully automatic. The user may, however, control the process in three different stages: the choice of f, the granularity of the decomposition, and the optimization criteria for the parameterization of each primitive. As surveyed in [14], different mapping functions capture different features of the shape, and the user could choose the most appropriate one according to the morphological complexity of the shape or to the application. The use of the Reeb quotient space ensures the minimal number of charts with respect to the number of critical points; however, the user could further segment the primitives of S_M to produce a finer segmentation, and therefore control over the skeleton, where required. Finally, the user could select any other criteria for optimizing the parameterization, even a different one for each cell, as the zippering of the parameterization is highly simplified by the connectivity of the patches. The generality of the approach, indeed, enables to adapt the segmentation to the parameterization distortion of each patch, and to choose any other embedding of the charts.

The paper is organized as follows. In Section 2, we briefly describe the segmentation of surfaces with an arbitrary genus based on the Reeb quotient space, define its coding as a shape graph and discuss the properties of the graph. In Section 3, the parameterization of the graph nodes is presented, and its application to remeshing are detailed in Section 4. Improvements and future work on global parameterization conclude the presentation of the proposed framework.

2. Topology-Driven Shape Graph

Differential topology provides a suitable framework for formalizing and solving several problems related to shape understanding and provides a powerful link between critical points, their configuration and the global properties of the shape. In particular, the notion of quotient space defined by Reeb in [15] can be used to define a canonical decomposition of a manifold into topological cells, given a continuous real-valued mapping function.

2.1. Reeb Graph and its Extension

Let M be a 2-manifold and $f : M \mapsto \mathbb{R}$ a mapping function. The *Reeb graph* R_G of M with respect to f is the quotient space of $M \times \mathbb{R}$ defined by the relation '$\sim$' with

$$(p, f(p)) \sim (q, f(q)) \leftrightarrow f(p) = f(q)$$

and p, q belong to the same connected component of $f^{-1}(f(p))$.

Intuitively, the Reeb quotient space collapses into a single point each connected component of the level set of f. While the previous definition does not make any hypothesis on the differentiability of the mapping function, if f is at least $C^2(M)$, Morse theory guarantees that the topological changes of the contours occur only at the critical values of f, and the Reeb quotient space is represented by a graph whose nodes correspond to critical values and whose arcs code the evolution of contours. Other applications of the Reeb graphs are presented in [13,18,19].

As thoroughly discussed in [20], the same relation between Reeb graph nodes and critical points exists also for triangle meshes analyzed with C^0 mapping functions. Other approaches to the characterization of discrete surfaces use local point-wise criteria to detect and classify critical points, by simulating the concept of critical point using the connectivity of the mesh as underlying topological space [21,22]. Two drawbacks can be identified: first, these methods rely on the hypothesis that all edge-adjacent vertices have different height; second, the number of the detected critical points is usually very high and pruning or simplification steps are necessary to make the resulting structures meaningful. Another solution is to simply observe that the contour levels decompose M into a set of regions, whose boundaries contain complete information for detecting critical areas and for classifying them as maximum, minimum and saddle areas. For example, if a contour does not contain any other contour and the value of the function on it is higher than the successive one, then the contour identifies a maximum area for the chosen function f. Following this idea, an extension of the Reeb definition has been proposed in [20] for continuous mapping functions defined over manifold triangle meshes, which yields to a shape segmentation with very good properties from the point of view of atlas generation.

Let $f : M \mapsto \mathbb{R}$ be a real mapping function defined on a manifold M, $[f_{\min}, f_{\max}]$ an interval containing $f(M)$, and $f_{\min} =: f_0 < f_1 < \cdots < f_n < f_{\max} =: f_{n+1}$ the distribution of the values of the contour levels $C_f(M)$, which are supposed to be all nondegenerate contours. A contour is *degenerate* if it is exactly at the position of a critical value; in this case, it is always possible to slightly change that value and get a nondegenerate contour. In addition, let $I = \{(f_i, f_{i+1}), i = 0, \ldots, n\} \cup \{f_{min} = f_0, f_1, \ldots, f_n, f_{\max} = f_{n+1}\}$ be the partition of the interval $[f_{\min}, f_{\max}]$ provided by the set of the $n + 1$ open interior parts of $[f_{\min}, f_1, \ldots, f_n, f_{\max}]$ and the function values of the contour levels.

Definition 1. *The Extended Reeb equivalence between two points $p, q \in M$ is given by the following conditions:*

(1) *$f(p)$ and $f(q)$ belong to the same element of $t \in I$;*
(2) *p, q belong to the same connected component of $f^{-1}(f(t)), t \in I$.*

© The Eurographics Association and Blackwell Publishing Ltd 2004

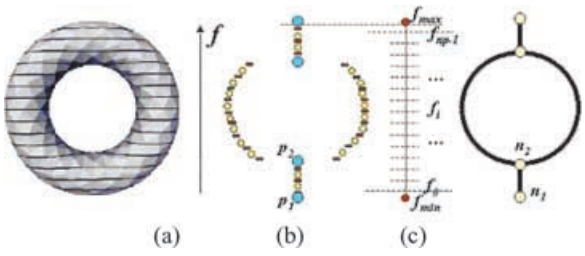

Figure 1: *(a) and (b) The quotient space induced by f, and (c) its graph-like representation. Connecting points are depicted by using red rectangles while normal points are shown as circles; circles represent the quotient of a region, while rectangles are images of contour levels.*

Therefore, by applying the notion of the quotient relation in 1, it follows that all points belonging to a region R are Reeb-equivalent in the extended sense and they may therefore collapse into the same point of the quotient space. The quotient space obtained from such a relation is a discrete space, which is called *Extended Reeb* quotient space (*ER*). Details on the characterization of the critical areas can be found in [20].

To represent the *ER* quotient space as a graph, the classes which are defined by points on contours are represented by *connecting points*, while all other classes are represented by normal points, simply called points (see Figure 1(b)). Connecting points are representative of contours and normal points are representative of regions. A point p representing a region R is adjacent through a connecting point to another point q representing another region R' in the quotient space, and a normal point is adjacent to as many connecting points as the number of connected components of the border of the associated region. From this point of view, the image of a regular region of M in the *ER* quotient space is adjacent only to two connecting points. Therefore, the connectivity changes of the graph representation are concentrated in the image of the critical areas, and they are equivalent to the standard Reeb graph representation which can be easily derived by merging the intermediate nodes representing regular areas into a single arc; in Figure 1(b), normal points that correspond to critical areas are depicted in orange. After this merging step, the *ERG* (*Extended Reeb Graph*) simply consists of nodes representing critical areas and the associated connecting arcs. In Figure 1, an example of the Extended Reeb quotient space is shown for a torus with respect to the height function f; in particular, the sequence of points between p_1 and p_2 of the quotient space *ER* in (b) represents an arc between the nodes n_1 and n_2 in (c).

2.2. Shape Segmentation Based on the Extended Reeb Equivalence

Based on these concepts, it is possible to define the segmentation of the input surface M into three types of primitives (i.e. cones, cylinders and bodies) each represented by regions with specific topological properties. First of all, our aim is to partition the input surface into a family of m patches $R_1, \ldots, R_m$ such that:

- $\bigcup_{i=1}^{m} R_i = M$;
- R_i is a connected region, $i = 1, \ldots, m$;
- $R_i^\circ \cap R_j^\circ = \emptyset$, $i \neq j$, with X° internal part of X;
- $R_i \neq \emptyset$ has 0-genus, and k_i boundary components $\{\gamma_j\}_{j=1}^{k_i}$.

Using the notion of Extended Reeb equivalence and the structure of the corresponding graph, we define these primitives as follows:

- A *cone* primitive is defined for each terminal node of the *ERG*, by merging the regions associated to the terminal node and all the normal regions associated to the arc connecting the terminal node to its adjacent one;
- A *cylinder* primitive is related to each arc connecting to inner nodes of the *ERG*, by merging all the regions associated to the arc connecting the two inner nodes;
- A *body* primitive is defined for each critical region associated to an inner node, containing a saddle point of the *ERG*.

The most important point is that each primitive $\{R_i\}_i$ has 0-genus, but a different number of boundary components. More precisely, a *cone* primitive has only one boundary component by definition, it identifies a critical region containing either a maximum or minimum, and it covers the portion of the shape until it meets the next critical region.

A *cylinder* primitive has two boundary components, and it either corresponds to a degenerate maximum or minimum (e.g. a volcano rim) or it simply corresponds to the part of the mesh that connects two critical regions.

Finally a *body* primitive may have k boundary loops, with $k \geq 3$, and it corresponds to a critical region containing a saddle point.

The correctness of the chosen primitives, i.e. their topological equivalence, is based on the fact that the topological type of a patch R_i depends only on the number of its boundary components and on the genus of the surface $R_i^\star$ obtained by gluing a disk to each loop γ_j, $j = 1, \ldots, k_i$. The general case is detailed by the following theorem [17].

Theorem 1. *Let M_1 and M_2 be two compact bordered surfaces; assume that their boundaries have the same number of components. Then, M_1 and M_2 are homeomorphic if and only if the surfaces $M_1^\star$ and $M_2^\star$, obtained by gluing a disk to each boundary component, are homeomorphic.*

© The Eurographics Association and Blackwell Publishing Ltd 2004

While the properties of the segmentation are completely independent of the chosen mapping function f, different f functions generate different decompositions and this allows to adapt the decomposition to the characteristics of the specific shape. We briefly review three possible choices for the construction of the *ER* graph to give an idea of the kind of decomposition they produce.

Reeb graph with respect to the distance from the barycenter. The distance function of the surface vertices from a given point p of the Euclidean space, $f_p(x) := \|p - x\|_2$, $x \in M$, represents a class of Morse functions. The point p could belong to the mesh or not, even though a reasonable choice is the barycenter of the surface which is easily calculated and, due to its linear dependence on all the vertices, stable to small perturbations.

Reeb graph defined by the topological distance from curvature extrema. In [23,24], a multiresolution curvature evaluation locates seed points p_i of high-curvature regions C_i, $i = 1, \ldots, s$ which are sequentially linked by using the topological distance on the simplicial complex, in a way similar to the wave-traversal technique [25].

Reeb graph induced by the geodesic distance. In [18], for each vertex of a mesh M, the value of the function f is given by

$$f(x) := \sum_i g(x, b_i) \cdot \text{area}(b_i),$$

where $g(x, b_i)$ represents the geodesic distance between x and b_i, $\{b_i\}_i$ is the set of the base vertices for the Dijkstra's algorithm that are scattered almost equally on the surface, and area(b_i) is the area of the 1-star of b_i.

The use of these primitives enables to segment M in a more natural way with respect to [4,5], while maintaining their parameterization and distortion control at a simple level. The factors which mainly differentiate this decomposition from simplification-based segmentation are the geometry of the allowed patches and their connectivity relations. We explicitly underline that each boundary component is shared by only two distinct patches, while in previous methods corner vertices on the common boundaries have an arbitrary number of incident regions, thus preventing to perform a regular remeshing. Because we deal with a simplified situation on the adjacency between patches, we guarantee a regular remeshing on the whole surface with the exception of localized vertices (see Section 4). The proposed surface segmentation is *minimal* with respect to the number of critical and regular regions which depends only on the genus of M and on the values of f on M. An adaptive segmentation guided by the parameterization distortion is detailed in Section 3.3.

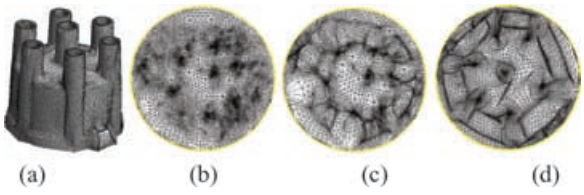

Figure 2: *(a) Input triangulation, parameterization with (b) constant, (c) least-square and (d) shape-preserving weights.*

3. Parameterization of Triangle Meshes with an Arbitrary Genus

The parameterization of 2-manifold meshes with one boundary and 0-genus has deserved great attention in research and the methods proposed reached a mature stage, some of them being a kind of standard now. One of the best known, called barycentric mapping, was introduced by Tutte [3] and studied by several authors [1,2].

In the following, we will describe this method and the proposed extension to handle an arbitrary number of boundary components. While the barycentric mapping has been used in our approach, all the other parameterization alternatives would work fine as well. We briefly overview some of them for the sake of completeness.

Parameterization based on barycentric-coordinates. The method proposed in [2,3] defines a global parameterization for a 2-manifold mesh M with one boundary and 0-genus. The homeomorphism φ between M and its convex parameter domain $\Omega \subseteq \mathbb{R}^2$ is the solution of the linear system

$$(I - W)u = b_x, \quad (I - W)v = b_y, \tag{1}$$

where the entries of W are defined as

$$\begin{cases} w_{ij} > 0, & \text{if } e = (i, j) \text{ is an edge of } M, \\ w_{ij} = 0, & \text{else,} \end{cases}$$

the vector b is a linear combination of the coordinates of the vertices in $\partial\Omega$, and $\sum_j w_{ij} = 1, \forall i$.

By allowing each internal vertex of Ω to be any convex combination of its neighbors, the procedure provides all possible valid planar embeddings of the graph T associated to M. The choice of the weights w_{ij} (i.e. constant, least-squares or shape-preserving) affects the distortion of the parameterization (see Figure 2); therefore, they have to be chosen in order to minimize the triangle deformation with respect to the geometry of the 3D mesh. In this way, all those tasks such as texture mapping, remeshing and approximation with continuous surfaces are performed on the planar domain instead of M.

In [26], the drawback of mapping the boundary of the 3D mesh onto a convex planar curve has been solved by using a multilayered virtual boundary. Finally, the method of

© The Eurographics Association and Blackwell Publishing Ltd 2004

barycentric-coordinates has been extended in [11] to the case of closed manifold triangle meshes with 0-genus, defining all its possible spherical parameterizations.

Parameterization based on energy minimization. Suppose the boundary vertices have been chosen and are fixed, then the previous framework is equivalent to a minimization problem [2] where the weights $(w_{ij})_{ij}$ define the functional

$$F(p_1, \ldots, p_N) := \sum_{(i,j)\text{edge}} w_{ij} \| p_i - p_j \|_2^2,$$

and whose minimum is the parameterization (Ω, φ). *Conformal* [8,27], and *harmonic weights* [28] represent alternative choices. In the first case, the aim is to improve the orthogonality and homogeneous spacing of the parameterization, while in the second one the distortion is controlled by minimizing a deformation energy. However, the standard discretization of harmonic functions does not always guarantee a one-to-one mapping.

In [29], Minkowsky functionals of 2-manifolds (i.e. area, Euler characteristic, and perimetry) are used for defining an intrinsic parameterization which is invariant to rotation and translation, and minimizes the distortion defined as the linear combination of the Dirichlet [28] and χ-energy. An angle-based flattening method which minimizes the relative distortion of the planar angles with respect to their 3D counterparts has been proposed in [30]. Finally, in [31] the parameterization is achieved by minimizing the Dirichlet energy of the triangulation without fixing in advance its boundary which evolves according to the optimization process.

3.1. Parameterization of Primitives

In this section, the method of barycentric-coordinates is extended to the case of a surface triangulation M with 0-genus and k simply-connected boundary components $\{\gamma_i\}_{i=1}^k$.

First of all, conical primitives, i.e. for $k = 1$, fall into the standard case and they are parameterized by solving the Equation (1) with shape-preserving weights.

We now analyze the case $k \geq 2$ (see Figure 3). Chosen one boundary component γ_1 (for example the one with the greater number of vertices or length), we parameterize M with respect to γ_1, that is, we consider the vertices of the remaining boundary components as unknowns in the linear system (1). In this way, we achieve a parameterization ϕ: $M \mapsto \Omega'$ where Ω' is a planar domain with k convex loops $\{\beta_i := \phi(\gamma_i)\}_{i=1}^k$. Clearly, we have a different ϕ for each chosen loop γ_i. In the case of the shape-preserving parameterization, we associate least-square weights to those vertices which belong to the boundary components $\{\gamma_i\}_{i=2}^k$ because they do not have a closed 1-star.

Another choice, which resembles the statement of Theorem 1, consists of closing $(k-1)$ boundary components of M, thus defining a new surface triangulation $M^\star$ with just one boundary, mapping $M^\star$ to Ω', and then removing the closed loops; we discard this method because the internal loops of the planar parameterization are generally nonconvex.

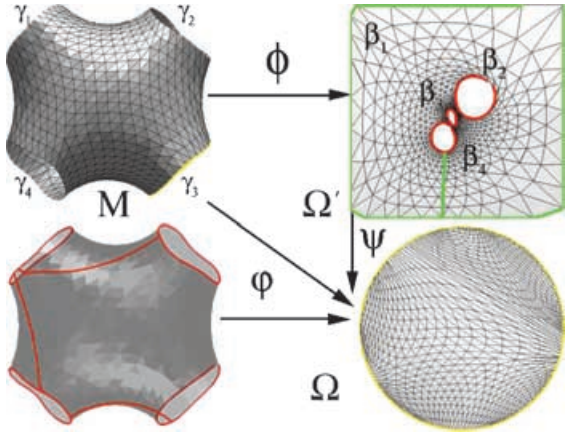

Figure 3: *General framework for the parameterization of a surface patch with $k = 4$ boundary components.*

Moreover, even if Ω' is homeomorphic to the input mesh, this approach is not useful for texture mapping, especially when the texture is nonuniform. In this case indeed, the entire image should be mapped onto the surface and not a part of it only. For remeshing applications or uniform textures, the presence of holes is simply solved by avoiding operations on them. For the removal of the internal closed curves $\{\beta_i\}_{i=2}^k$ (as detailed in Sections 3.1.1 and 3.1.2), we define a new planar domain Ω with only one boundary and a homeomorphism $\psi : \Omega' \mapsto \Omega \subseteq \mathbb{R}^2$ with the following properties:

- The boundary $\partial\Omega$ of Ω is convex;
- Each internal boundary component β_i of Ω' is mapped to a curve $\psi(\beta_i)$ of $\partial\Omega$, $i = 2, \ldots, k$.

We now detail the steps of the algorithm distinguishing the case $k = 2$ (i.e. parameterization of cylindrical primitives), and $k \geq 3$ (i.e. parameterization of bodies).

3.1.1. Parameterization of Cylindrical Primitives

If $k = 2$, the surface triangulation is topologically equivalent to a cylinder and the parameterization ϕ: $M \mapsto \Omega'$ embeds M onto a domain Ω' with two boundary components $\beta_1 := \phi(\gamma_1)$ and $\beta_2 := \phi(\gamma_2)$. Let p and q be the closest points, with respect to the Euclidean distance, on β_1 and β_2; that is,

$$\| p - q \|_2 \equiv \min_{r \in \beta_1, s \in \beta_2} \{ \| r - s \|_2 \},$$

and $[p, q]$ the line segment from p to q (see Figure 4(a) and (b)).

© The Eurographics Association and Blackwell Publishing Ltd 2004

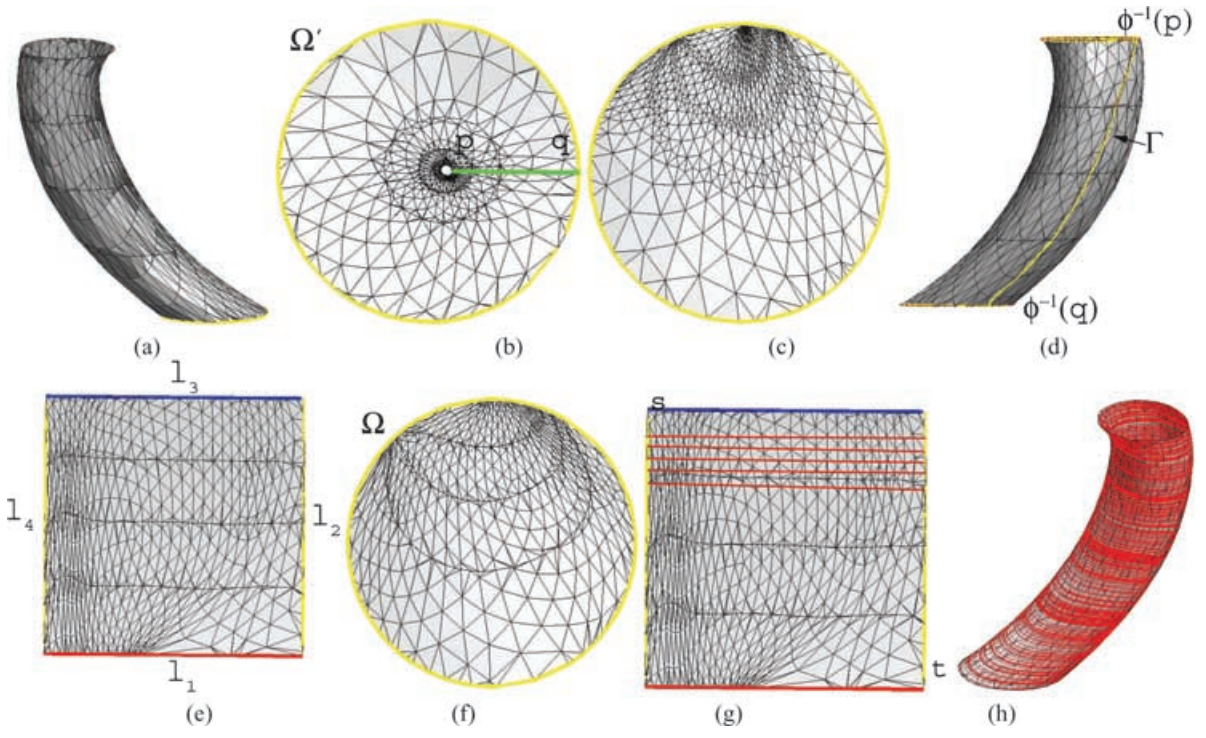

Figure 4: *(a) Input cylindrical surface R; (b) least-square parameterization of R with respect to the boundary depicted in yellow in (a), and minimal cut γ (green line); (c) shape-preserving unfolding of Ω' with respect to the depicted cut in (b); (d) 3D cut Γ; shape-preserving parameterization of R with respect to Γ on the (e) unit square and (f) on the unit circle; (g) coordinate lines on the square and (h) their counterparts on the cylinder. The example shows the stability of the cut identification and parameterization of R in spite of its high-curvature, irregular geometry and connectivity.*

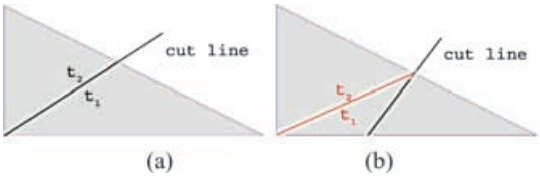

Figure 5: *(a) Cut of the triangle trough a vertex and (b) re-triangulation.*

The cut $[p, q]$ is inserted in the input triangulation before unfolding the parameter domain onto Ω. To this end, if $[p, q]$ intersects a triangle t passing through one of its vertices t is split into two new faces t_1 and t_2 which share a part of the cut (see Figure 5(a)). Otherwise, $[p, q]$ splits t into one triangle and a quadrilateral q; then, q is re-triangulated by subdividing it along its shortest diagonal (see Figure 5(b)). This update is also performed on the 3D triangulation in order to ensure that M and Ω' share the same topology.

Successively, we cut Ω' along $[p, q]$, thus unfolding Ω' to Ω through ψ. The unfolding map ψ is achieved by duplicating the cut $[p, q]$ to $[q, p]$, converting β_1, β_2 and the cuts into one connected loop $\{\beta_1, [p, q], \beta_2^{-1}, [q, p]\}$, and applying the Floater's parameterization (see Figure 4(c)). Each closed curve γ has an anticlockwise orientation; γ^{-1} means that we have reversed the ordering of its vertices (i.e. clockwise orientation). Finally, the cut operation is coded into a relation $\mathcal{S}$ between $\psi([p, q])$ and $\psi([q, p])$. Therefore, the map $\varphi := \psi \circ \phi$ embeds M onto Ω.

The linear path $[p, q]$ exploited for mapping Ω' to Ω defines a curve $\Gamma := \phi^{-1}([p, q])$ on M; the more ϕ maintains the geometry of the input mesh the better the line connecting $\phi^{-1}(p)$ to $\phi^{-1}(q)$ approximates the corresponding geodesic (see Figure 4(d)). Alternatively to the previous approach, we can parameterize the cylindrical primitive directly using the 3D cut Γ without applying two consecutive unfoldings with the aim of avoiding to accumulate the distortion in the proximity of the boundary of Ω (see Figure 4(e–f)). We use this new embedding φ: $M \mapsto \Omega$ in all the following examples.

3.1.2. Parameterization of Bodies

We solve the case of k boundaries, with $k \geq 3$, by using an iterative procedure. Supposed that we have removed $(i - 1)$

© The Eurographics Association and Blackwell Publishing Ltd 2004

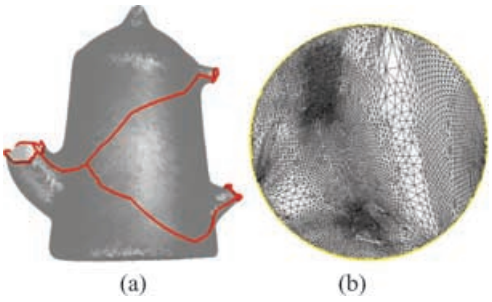

Figure 6: *(a) Body primitive extracted by using as f the geodesic distance from curvature extrema and (b) parameterized with respect to the cut shown in (a).*

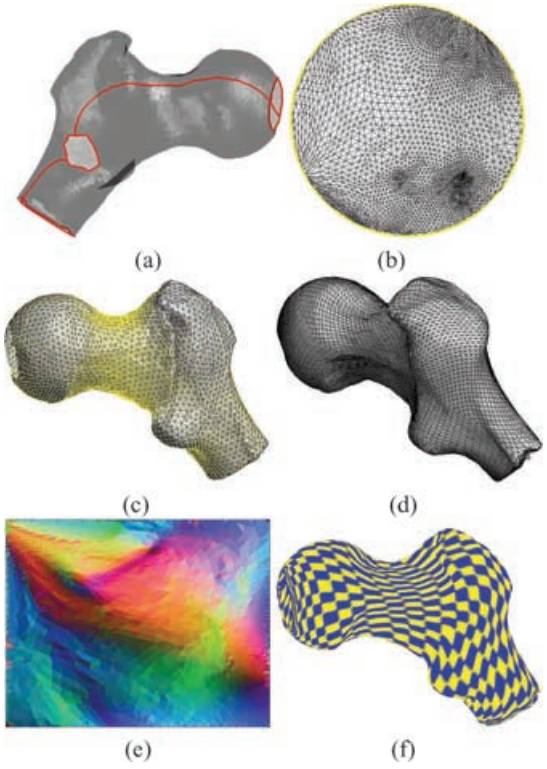

Figure 7: *(a) Cut on a surface of 0-genus with three boundary components, (b) unfolding onto the unit circle (shape-preserving weights), (c) regular sampling, (d) regular remeshing, (e) normal-map image (1024×1024) and [9], (f) texture mapping.*

boundary components, at the ith step we cut the current parameter domain Ω'_i along the line segment of minimal length which joins its external loop with the closest internal boundary component. If $\Omega'_1 := \Omega'$, let $\psi_i \colon \Omega'_i \mapsto \Omega'_{i+1}$ be the ith embedding; at the end of this process, the internal loops of Ω' are mapped onto $\partial\Omega'_k$ through the function $\psi := \psi_{k-1} \circ \cdots \psi_2 \circ \psi_1$ (see Figures 3, 6 and 7).

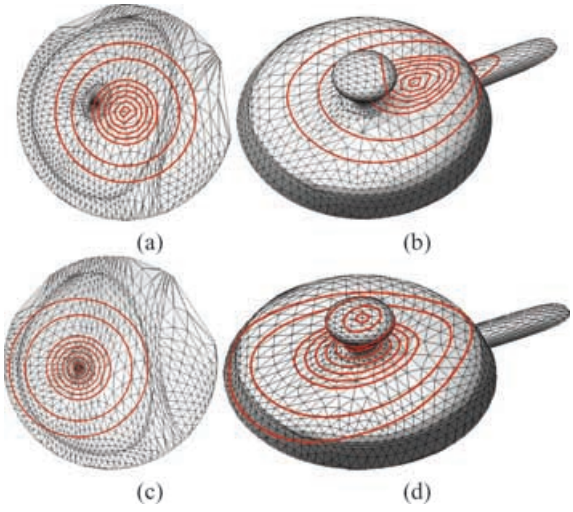

Figure 8: *(a) Set of concentric circles on the parametric domain, and (b) their corresponding curves on M; (c) and (d) sections with respect to the critical point (f is the height function).*

3.2. Shape Graph and Coding of the Parameterization

Throughout the previous sections we have identified and parameterized cylinders, cones and bodies achieving a segmentation of the input object and a parameterization of each building patch. The shape decomposition can be coded in an attributed graph S_M whose nodes are the extracted primitives, while the arcs code the adjacency relations among them.

Due to the properties of the topological decomposition, and parameterized each arc between two adjacent nodes either connects a cylinder to a body, or a cone to a body.

Based on the parameterization of each patch, the graph S_M can be augmented with additional geometric and structural information, namely the centerline skeleton of the shape computed patch by patch. The global skeleton is connected because the skeletal line of each primitive shares the barycenter of the common boundary components with the adjacent patch.

More in details, for extracting the skeleton Σ of a conical primitive (see Figure 8(a) and (b)), in the mapping step we consider as Ω the unit circle with a set of circunferences $\{S(0, r_i)\}_i$ centered in the origin and with radii $0 \leq r_i \leq r_{i+1} \leq 1$; then, Σ is built by joining the barycenters of the curves $\varphi^{-1}(S(0, r_i))$ on M. We can optimize the previous step by choosing $\varphi(p)$ as center of the circles, where p is a critical point of (M, f) (see Figure 7(c) and (d)).

For extracting the skeleton Σ of a cylindrical primitive, we choose as Ω the unit square $[0, 1] \times [0, 1]$ where the cuts

© The Eurographics Association and Blackwell Publishing Ltd 2004

$[p, q]$ and $[q, p]$ are mapped onto the line segments l_2, l_4, while the two boundary components β_1 and β_2 are identified with l_1 and l_3 respectively (see Figure 4(g)). First of all, we associate to the primitive a *coordinate network* of lines; each loop is achieved as $\varphi^{-1}(\{s = constant\})$ and each parallel as $\varphi^{-1}(\{t = constant\})$. Then, each loop is collapsed to its barycenter thus defining a skeletal line whose number of nodes can be refined by increasing the number of loops in spite of the mesh density and connectivity [23] (see Figure 4(h)). The coordinate network is useful for visualizing the presence and location of distortions induced by the parameterization and due to the selection of a specific set of weights in (1) or to a particular cut (e.g. along feature lines [32]) for the unfolding. Finally, Γ and a section $\varphi^{-1}(\{s = constant\})$ represent the topological generators of the cylindrical patch.

We explicitly underline that chosen a conical (respectively cylindrical) primitive R embedded by φ: $M \mapsto \Omega$, its skeletal line Σ is *aligned with the parameterization* in the sense that Σ is the Reeb graph of R with respect to $f(x) := \|\varphi(x)\|_2, \forall\, x \in M$ (resp. $f(x) := pr_2(\varphi(x)), \forall\, x \in M$, with $pr_2(t, s) = s, \forall (t, s) \in \mathbb{R}^2$). This property enriches existing methods based on the Reeb graph [33] with the information and applications of parameterization; we thus provide a tool which uses topology for the patch decomposition and geometry for the parameterization. Finally, for body primitives we simply consider as skeleton the lines connecting the center of mass of the body to the barycenters of its boundary components.

S_M, augmented with the centerline skeleton, gives a high-level geometric and topological knowledge on where and how regions are located and glue together; also, S_M specifies how we can generate the input surface with the building primitives (or equivalently, with their planar embeddings) extracted by using the Reeb graph. Moreover, the S_M stores information on the size and generators of cylinders and cones.

Starting from the partition $\{R_i\}_{i=1,\ldots,m}$ of M parameterized by $\varphi_i : R_i \mapsto \Omega_i$, $i = 1, \ldots, m$, the *graph-based parameterization* of M is the collection $\mathcal{P} := \{(R_i, \varphi_i, \Omega_i)\}_{i=1,\ldots,m}$ enriched with the adjacency relations among primitives coded by the shape-graph. Equivalently, we substitute each node of the shape-graph with the parameterization of the corresponding primitive calculated by using standard (e.g. cones) or specialized methods (e.g. cylinders and bodies). See Figure 9 for a complete view of the parameterization graph and Figure 10 for more complex surfaces. An example of local deformations is shown in Figure 11.

3.3. Adaptive Approach to Shape Decomposition and Parameterization

We deal with complex 3D shapes in a more flexible way through an adaptive implementation of the previous method

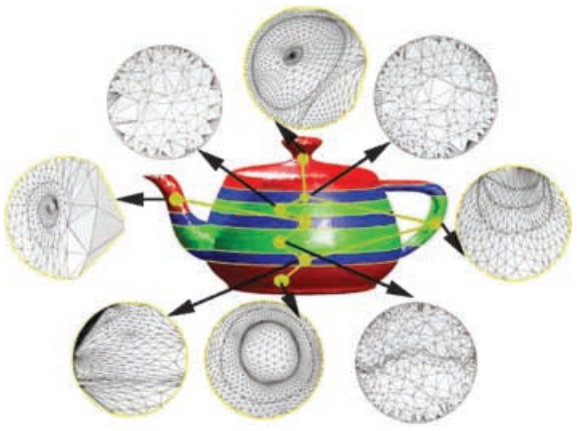

Figure 9: *Shape-graph and parameterization of the building primitives related to the minimal segmentation induced by the Reeb graph with respect to the height function.*

which slices the surface in correspondence of topological changes and where high parameterization distortions or curvature extrema [24,34] occur. To this end, after the identification of the regions $\{R_i\}_{i=1,\ldots,m}$ we proceed as follows. For each patch R_i,

(1) We locate its subregions S with high L^2, or L^∞ [42] stretch (resp. multi-resolutive curvature [24]);
(2) We use the averaged value $\overline{\alpha}$ of f on its boundary components to define the corresponding iso-contour $f^{-1}(\overline{\alpha})$ on R_i;
(3) We subdivide R_i in correspondence of the new contours (if any).

The type of each new subpatch can be different with respect to that of R_i, but it always falls in the previous classification of the building primitives. In this way, the refined segmentation of M enables to reduce the distortion of the parameterization; alternative criteria can be introduced with the unique constraint of defining 0-genus patches. In Figures 10(a) and 10(b) and 11 the minimal and adaptive segmentation are shown. Table 1 gives the number and type of primitives of the segmented surfaces related to the examples shown in the paper.

4. Remeshing

The advantages of using the proposed method for remeshing are discussed in this section. To this end, we review the remeshing techniques commonly used to approximate a given surface M with a new triangulation $\overline{M}$ which has a specific connectivity (i.e. regular, semi-regular) and geometry (i.e. anisotropic, isotropic vertex sampling).

© The Eurographics Association and Blackwell Publishing Ltd 2004

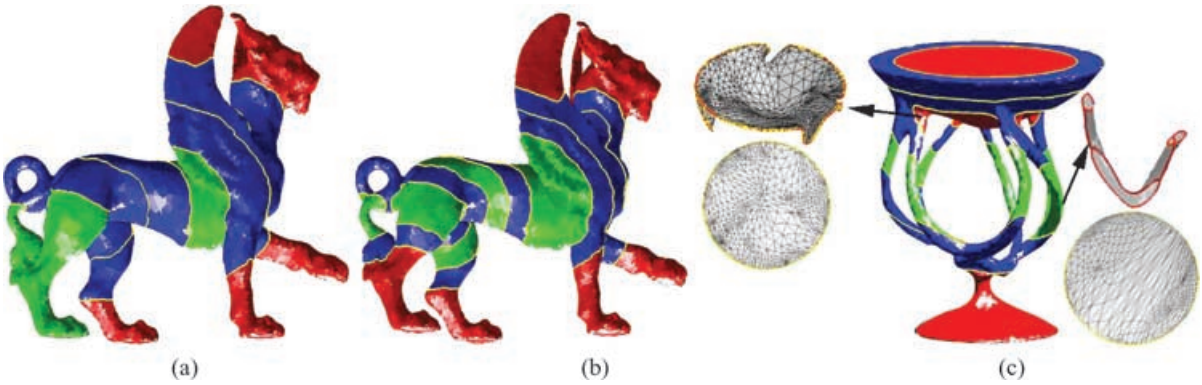

Figure 10: *(a) Minimal and (b) adaptive segmentation of the feline (f is the geodesic distance from curvature extrema), (c) local segmentation of a complex shape of genus seven (f is the distance from the barycenter).*

Figure 11: *(a) Minimal decomposition with respect to the height function and (b) adaptive segmentation induced by the parameterization distortion.*

Table 1: *Number of patches of the segmentation.*

Surf.	Fig.	No. of Patch	No. of Cones	No. of Cyl.	No. of Bodies
Teapot	9	9	3	3	3
Bitorus	12	15	4	6	5
Feline	10(a)	12	6	2	4
Feline	10(b)	17	7	4	6
Vase	10(c)	25	14	7	4

Given a disk-like surface M parameterized by φ: $M \mapsto \Omega$, a *regular remeshing* [35,36] defines a base mesh S^0 with a minimal number of triangles which are subdivided to obtain a sequence $S^0, S^1, \ldots, S^r$ of triangulations with subdivision connectivity and contained in Ω. The iteration proceeds until S^r (respectively $\varphi^{-1}(S^r)$) is a good approximation of Ω (respectively M) with respect to some geometric error (e.g. L^2 norm). Therefore, this method uses the same number of samples on the parametric domain in spite of the presence in Ω of triangles with a different area. As a result, we have an oversampling of those triangles with a greater area and an undersampling in regions where small local features are located. To overcome this drawback, two strategies are available. The first one consists of re-parameterizing Ω to a new domain $\overline{\Omega}$ with the aim of equalizing the area of each triangle; internal vertices are updated using an area-based smoothing [36] or a relocation strategy [37]. This optimization step can produce inverted triangles and in the case of small features it does not avoid the necessity of a large number of subdivision steps.

To overcome the exponential growth of the number of vertices, the second choice is an *adaptive remeshing* $(S^k)_k$ of Ω which localizes on the current remesh S^k those triangles where the approximation error between M and $\varphi^{-1}(S^k)$ exceeds a given error ε and which have to be split [5]. A triangle $t \in S^k \subseteq \Omega$ is subdivided if the following condition

$$E(t) := \max_{p_i \in t,\, p_i \in \Omega} \left\{ dist(\varphi^{-1}(p_i), \pi) \right\} > \varepsilon$$

hold, where π is the plane defined by the triangle $\varphi^{-1}(t)$. After this phase, the mesh S^{k+1} is achieved from S^k by using the red-green triangulation. The iteration terminates when the local error $E(t)$ does not exceed ϵ for all $t \in S^r$; finally, $\varphi^{-1}(S^r)$ is evaluated combining the point plane location and barycentric coordinates.

Local remeshing [5,35,38] is based on partitioning 3D meshes into disk-like patches, each one parameterized and then remeshed. Main problems of this approach are the lack of symmetry in the patch decomposition and the dependence of its structure from the simplified mesh M_S which defines the atlas identification. The regular connectivity of each patch cannot be extended to the entire mesh and extraordinary vertices are 'randomly' located on the remeshed surface $\overline{M}$.

Global remeshing [9,36,39] re-samples the global parameterization of M with a regular or an adaptive grid and thus treats the original mesh as a whole while guaranteeing the regularity of the connectivity. The problems which affect the definition of a 'good' global parameterization, i.e. the choice of the cuts for the unfolding of surfaces with an arbitrary

© The Eurographics Association and Blackwell Publishing Ltd 2004

genus and the parameterization distortion of regions with a high-curvature, are reflected on the final result.

An alternative to both approaches is to work directly on the surface with an iterative procedure which modifies local regions on M [37,40], usually the 1-star of each internal vertex, and controls their smoothness and sampling rate. This *mesh adaptation process* reduces the computational cost and avoids the drawbacks of decomposing and cutting M; however, the locality of the approach does not guarantee to avoid error accumulation through feature lines and to effectively optimize the sampling of the original surface.

4.1. Feature-Based Local Remeshing

We apply the graph-based parameterization for the remeshing of a 3D shape with an arbitrary genus and density. As refinement operator for uniform remeshing we consider the 1-to-4 operator that recursively subdivides each triangular face into four subtriangles by introducing three new vertices on the edges. In this way, each remeshed patch has an implicitly defined connectivity which is exploited in several tasks such as compression, progressive transmission and multiresolution editing. The adaptive remeshing is based on the method presented in [5].

We first discuss how each primitive is remeshed by taking into account their different parameterizations and then combined to give a coherent and global remesh of the input surface.

Remesh of conical primitives. Because $S^r \subseteq \Omega$, we ensure the remeshing of $\partial\Omega$ by projecting ∂S^r onto $\partial\Omega$; to this end, we map each vertex $p \in \partial S^r$ to the point of intersection between the segment $\{\lambda p\colon \lambda > 0\}$ and $\partial\Omega$. Once computed S^r, the remeshed data set $\overline{M}$ is achieved as $\varphi^{-1}(S^r)$; each vertex $p \in S^r$ is written using its barycentric-coordinates with respect to the vertices of a triangle $t := (i, j, k) \in T$ which contains it, i.e.

$$p = \alpha v_i + \beta v_j + \gamma v_k, \quad \alpha + \beta + \gamma = 1,$$

whose 3D counterpart is $\varphi^{-1}(p) = \alpha\varphi^{-1}(v_i) + \beta\varphi^{-1}(v_j) + \gamma\varphi^{-1}(v_k)$. The remeshing is reduced to a point-location problem in an irregular triangulation whose computational cost is $O(\sqrt{N})$ (see Figure 12(a–d)).

Remesh of cylindrical primitives. For a cylindrical primitive M, we can proceed in two different ways. As first choice, we apply the previous approach with its parameterization φ: $M \mapsto \Omega$ onto the unit square; the edges l_2 and l_4 have to be coherently re-sampled (i.e. $(1, \alpha) \in l_2$ if and only if $(0, \alpha) \in l_4$, $0 \leq \alpha \leq 1$), in order to ensure that $\varphi^{-1}(l_2)$ and $\varphi^{-1}(l_4)$ coherently join when mapped back to $\Gamma \subseteq M$. In the case of uniform remeshing, the vertices of $\partial\Omega$ have 3-connectivity and each vertex on $\varphi^{-1}(l_2)$ has 6-connectivity. Therefore, the remeshed patch has 6(respectively 3)-connectivity for internal (respectively boundary) vertices and the number of vertices on the two remeshed boundary components is the same (see Figure 12(e)). An example of adaptive remeshing is given in Figure 12(f).

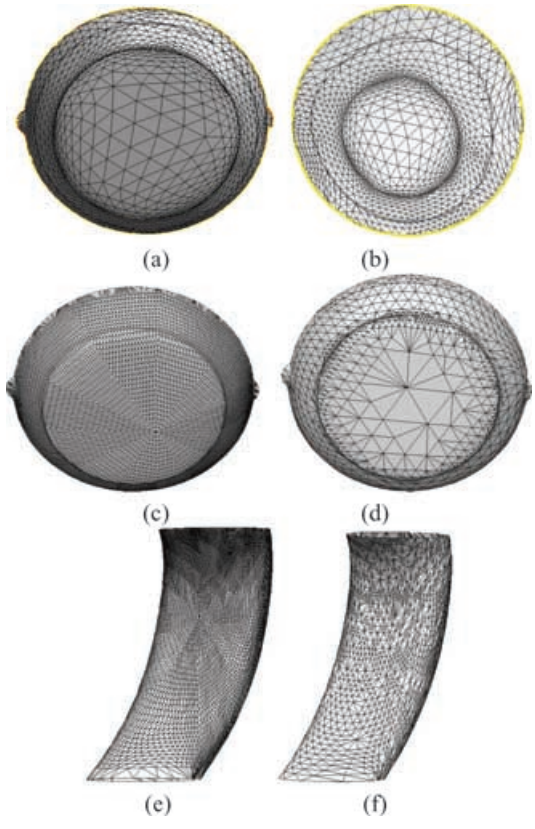

Figure 12: *(a) Input conical primitive, (b) shape-preserving parameterization, (c) regular and (d) adaptive remesh of (a). The examples (e) and (f) show the uniform and adaptive remesh of the cylinder in Figure 4.*

The second possibility is to use the embedding $\phi\colon M \mapsto \Omega'$ onto the unit circle with the boundary component β_2 in its interior. In this case, we take care of introducing in Ω' the intersection between β_2 and S^r, as done in Section 3.1.1. This procedure is preferred to the previous one when the parameterization of the cylindrical patch onto the unit square is strongly distorted by an irregular sampling of its geometry. We explicitly note that we cannot know in advance how many vertices of β_2 belong to S^r. The same considerations apply to bodies (see Figure 7).

We now consider what happens on the boundary components of adjacent patches in $\mathcal{P}$. If the same boundary component γ is used to parameterize two adjacent regions R_i, R_j (therefore $\gamma \subseteq R_i \cap R_j$), we consider the same orientation and starting point on it in order to ensure that it has the same parameterization for both regions. This choice guarantees that $\partial\Omega_i \equiv \partial\Omega_j$ and that the corresponding remeshed

© The Eurographics Association and Blackwell Publishing Ltd 2004

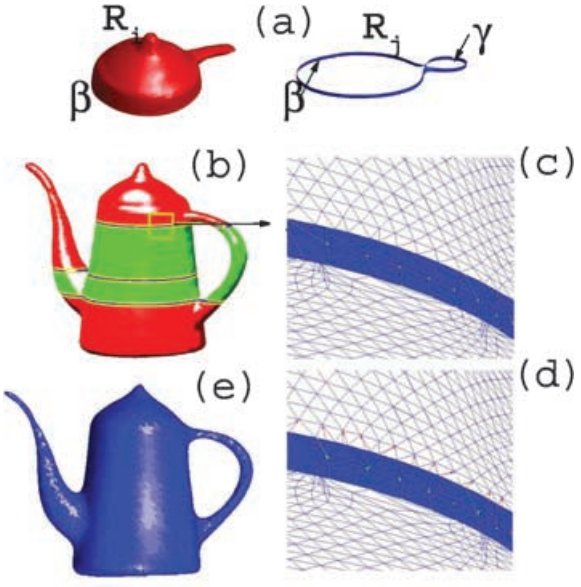

Figure 13: *(a) Adjacent patches (R_i is a conical primitive, and R_j is a body with four boundary components), (b) topological segmentation, remeshed data set (c) before and (d) after the update of the common boundary; (e) final result.*

regions (with respect to the same S^r) coherently join on the common (remeshed) boundary whose vertices have valence six.

Let us now consider the common boundary component β of two adjacent patches R_i and R_j, and suppose that one of them has been parameterized with respect to a loop $\gamma \neq \beta$ (see Figure 13(a)). In this case, their remeshed boundaries Θ_i, Θ_j in $\mathbb{R}^3$ corresponding to β do not coherently join even though they are two different descriptions of $\varphi^{-1}(\beta)$. Supposed that Θ_i has a greater number of vertices with respect to Θ_j, we substitute Θ_j with Θ_i (see Figure 13(b) and (c)) and we insert it into the remeshed patch corresponding to R_j (see Figure 13(d) and (e)). This choice is intended to minimize the number of extraordinary vertices, and we use this strategy if we consider a different r in S^r for each patch or the adaptive remeshing (see Figure 14). An alternative zippering of adjacent patches is discussed in [41].

In Table 2, we compare the L^2 and L^∞-stretch before and after the cutting of several 0-genus surfaces M; the values show that the embedding of M onto a parameter domain Ω has a distortion much smaller than the mapping onto Ω' obtained without removing the internal loops.

5. Conclusions and Future Work

The proposed framework defines a user-independent model for graph-based parameterization of 3D shapes into a minimal number of maximal charts, and it is associated to a centerline skeleton (aligned with the parameterization), which stores geometric information as node labels.

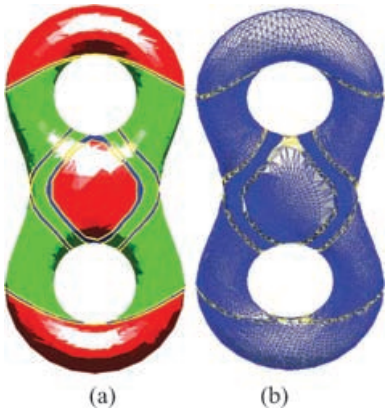

Figure 14: *(a) Shape segmentation with f Euclidean distance from the barycenter. (b) Uniform local remeshing of a bitorus; yellow curves locate boundary components between adjacent regions.*

Table 2: *Comparison of the parameterization stretch before and after the cut for patches of different shape and number of boundary components.*

Patch	Figure	$L^2(\Omega')$	$L^\infty(\Omega')$	$L^2(M)$	$L^\infty(M)$
body	3	32.91	147.74	29.86	12.34
cyl.	4	7.53	137.74	6.12	48.42
teapot	6	29.83	1039	16.08	619.50
bone	7	540.71	6764.45	26.01	906.67

The proposed patch identification locates regions, which are global features of the input shape; in fact, cones and cylinders represent protrusions, while bodies are junctions among them. This choice reduces the number of patches with respect to the atlas generation, and thus improves the regularity and smoothing of the remeshing through the boundaries of adjacent regions, which usually require a specific identification and treatment. The adaptive surface segmentation enables to reduce the distortion in the parameterization of each region R_i with benefits on the remeshing. Finally, the localization of extraordinary vertices is an improvement with respect to previous methods which do not control their location on the surface. Being N the number of vertices of M, the computational cost of the topological segmentation is $O(N \log N)$, and $O(N)$ that of the parameterization.

Our current improvement is the optimization of the remeshing in order to minimize the number of localized extraordinary vertices. The strategy under development exploits the red/green triangulation and consists of ordering the patch parameterization starting from their adjacency relations and common boundaries.

© The Eurographics Association and Blackwell Publishing Ltd 2004

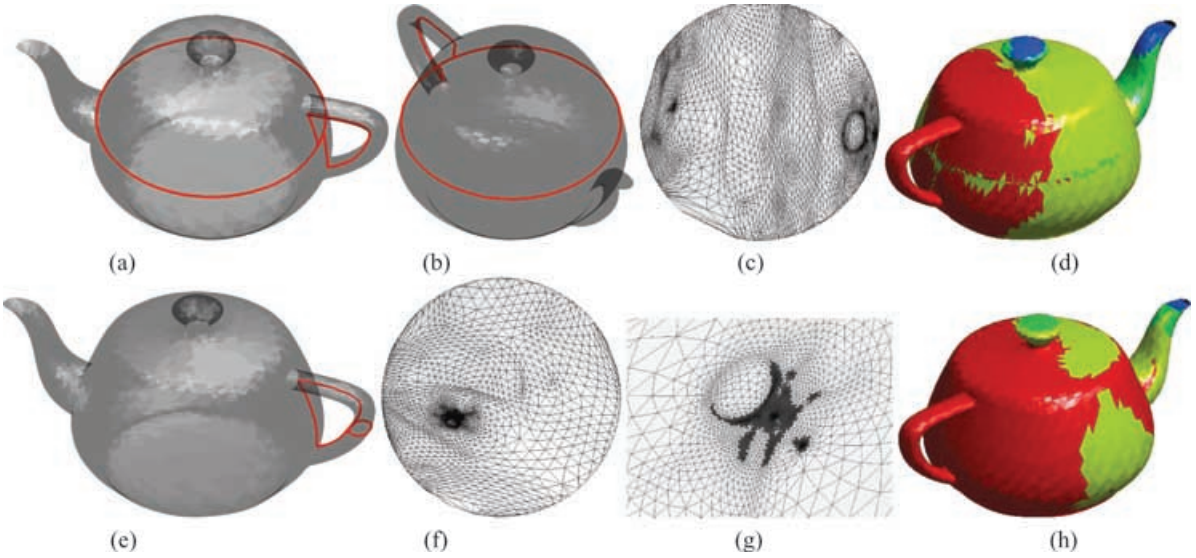

Figure 15: *Global parameterization with respect to two different unfoldings; the topological information provided by the Reeb graph with respect to the height function f is used to identify a handle on the input object. In the first (respectively second) row the handle is the body (a and b) (respectively handle (e)) of the teapot and it is cut by using an iso-contour γ of f. Duplicating γ, we have a surface $\overline{M}$ of 0-genus with two boundary components, that is a cylinder; the new cut and the unfolding of $\overline{M}$ are calculated as described in Section 3.1.1. The unfolding on the unit circle is shown in (c), (f) and (g) gives a zoom-in of (f). Each row shows the normalized L^2 stretch distribution s [42]. Firt row (d): $L^2(M) = 37.36$ where vertices are red if $0 \leq s \leq 0.001$, yellow if $0.001 < s \leq 0.005$, green if $0.005 < s \leq 0.2109$ and blue if $0.2109 < s \leq 1$. Second row (h): $L^2(M) = 388.85$, red if $0 \leq s \leq 0.001$, yellow if $0.001 < s \leq 0.0085$, green if $0.0085 < s \leq 0.2691$ and blue if $0.2691 < s \leq 1$. The cut achieved as pre-image of the line segment [p, q] is not affected by the high curvature of the handle and by the distortion of the parameterization used for its evaluation.*

The topological information provided by the Reeb graph, and the method used for parameterizing bodies defines a simple method for the global embedding of M into the plane (see Figure 15).

Because the model is based on a high-level representation of 3D shapes, the next goal is to perform shape transformations which affect the object geometry and supervised by a check of the topological meaningfulness of the editing operations (see Figure 16).

Acknowledgments

This work has been supported by the EC-IST FP6 Network of Excellence 'AIM@SHAPE'. Special thanks are given to Silvia Biasotti for providing the segmentation based on the Extended Reeb Graph and to the Shape Modelling Group at IMATI-GE/CNR.

References

1. M. S. Floater and K. Hormann. Surface parameterization: A tutorial and survey. In *Multiresolution in Geometric Modelling*, N. A. Dodgson, M. S. Floater and M. A. Sabin. (Eds.), Springer, 2004.

2. M. S. Floater. Parametrization and smooth approximation of surface triangulations. *Computer Aided Geometrical Design*, 14(3):231–250, 1997.

3. W. T. Tutte. How to draw a graph. *Proceedings of the London Mathematical Society*, 13, 743–768, 1968.

4. M. S. Floater, K. Hormann and M. Reimers. Parameterization of manifold triangulations. In *Approximation Theory X: Abstract and Classical Analysis*. Vanderbilt University Press, pp. 197–209, 2002.

5. A. W. F. Lee, W. Sweldens, P. Schröder, L. Cowsar and D. Dobkin. MAPS: Multiresolution adaptive parameterization of surfaces. *Computer Graphics 32*, Annual Conference Series, 95–104, 1998.

6. H. R. Boier-Martin and J. Jin. Parametrization of triangle meshes over quadriangular domains. In *Eurographics Symposium on Geometry Processing (SGP2004)*, Eurographics Association, pp. 197–207, 2004.

7. L. Kobbelt, S. Campagna and H.-P. Seidel. A general framework for mesh decimation. In *Graphics Interface*, pp. 43–50, 1998.

© The Eurographics Association and Blackwell Publishing Ltd 2004

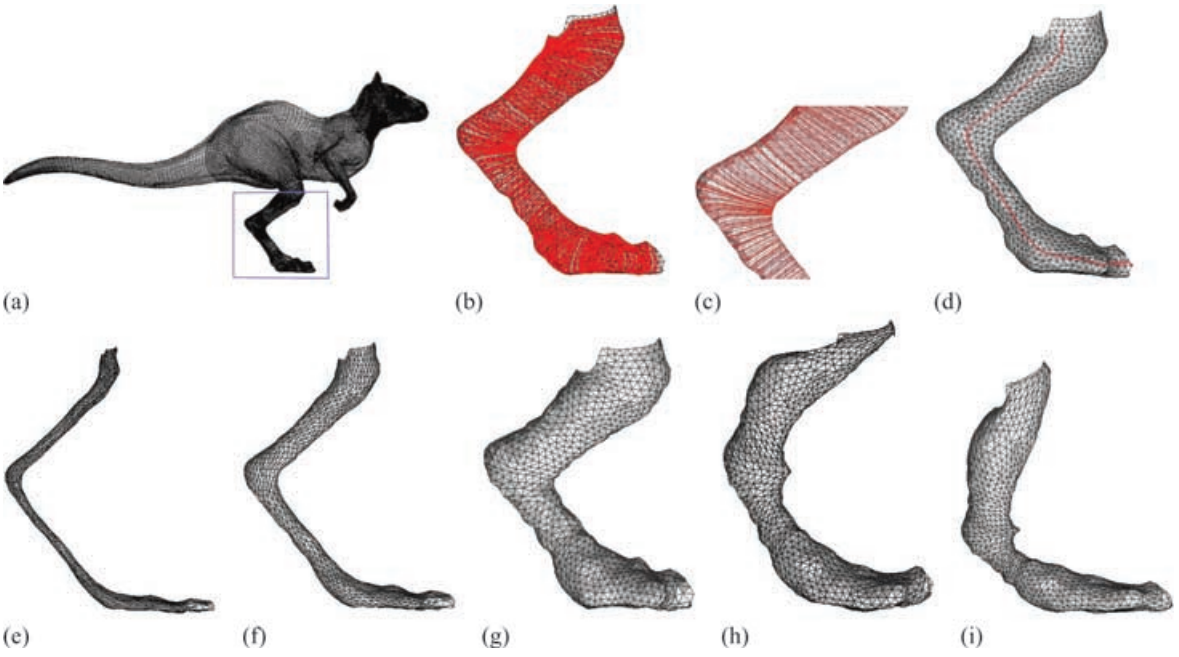

Figure 16: *(a) Conical primitive (blue box), (b) and (c) iso-contours induced by its parameterization, (d) skeletal line. (e–i) Deformations achieved by altering the skeleton in (d).*

8. B. Lévy, S. Petitjean, N. Ray and J. Maillot. Least squares conformal maps for automatic texture atlas generation. In *Proceedings of SIGGRAPH 2002*, vol. 21(3) pp. 362–371, 2002.

9. X. Gu, S. J. Gortler and H. Hoppe. Geometry images. In *Proceedings of the 29th Annual Conference on Computer Graphics and Interactive Techniques*, ACM Press, pp. 355–361, 2002.

10. X. Gu and S.-T. Yau. Global conformal surface parameterization. In *Proceedings of the Eurographics/ACM SIGGRAPH symposium on Geometry processing*, Eurographics Association, pp. 127–137, 2003.

11. C. Gotsman, X. Gu and A. Sheffer. Fundamentals of spherical parameterization for 3d meshes. *ACM Transaction on Graphics*, 22(3):358–363, 2003.

12. E. Praun and H. Hoppe. Spherical parametrization and remeshing. *ACM Transaction Graphics* 22(3):340–349, 2003.

13. S. Biasotti, S. Marini, M. Mortara and G. Patane. An overview on properties and efficacy of topological skeletons in shape modelling. In *SMI '03: Proceedings of Shape Modeling International 2003*, Los Alamitos, May 2003, M. Kim (Ed.), *IEEE Computer Society*, pp. 245–254.

14. S. Biasotti, S. Marini, M. Mortara, G. Patane, M. Spagnuolo and B. Falcidieno. 3D shape matching through topological structures. *Lecture Notes in Computer Science* 2886, 194–203, 2003.

15. G. Reeb. Sur les points singuliers d'une forme de pfaff completement integrable ou d'une fonction numerique. In *Comptes Rendu Acad. Sciences*, Sciences Park, pp. 847–849, 1946.

16. J. Milnor. *Morse Theory*. Princeton University Press, 1963.

17. M. P. DoCarmo. *Differential Geometry of Curves and Surfaces*. Prentice-Hall Inc., Englewood Cliffs, New Jersey, 1976.

18. M. Hilaga, Y. Shinagawa, T. Kohmura and T. L. Kunii. Topology matching for fully automatic similarity estimation of 3D shapes. In *Proceedings of the 28th Annual Conference on Computer Graphics and Interactive Techniques*, ACM Press, pp. 203–212, 2001.

19. Y. Shinagawa, T. Kunii and Y.-L. Kergosien. Surface coding based on Morse theory. *IEEE Computer Graphics and Applications*, 11(5):66–78, 1991.

20. S. Biasotti. *Computational Topology Methods for Shape Modelling Applications*. Ph.D. Thesis, Universitá degli Studi di Genova, May 2004.

© The Eurographics Association and Blackwell Publishing Ltd 2004

21. T. Banchoff. Critical points and curvature for embedded polyhedra. *Journal of Differential Geometry*, 1, 245–256, 1967.

22. H. Edelsbrunner, J. Harer, V. Natarajan and V. Pascucci. Morse-smale complexes for piecewise linear 3-manifolds. In *Proceedings of the Nineteenth Annual Symposium on Computational Geometry*, ACM Press, pp. 361–370, 2003.

23. M. Mortara and G. Patanè. Shape covering for skeleton extraction. *International Journal of Shape Modelling* 8(2):139–158, 2002.

24. M. Mortara, G. Patanè, M. Spagnuolo, B. Falcidieno and J. Rossignac. Blowing bubbles for the multi-scale analysis and decomposition of triangle meshes. *Algorithmica (Special Issue on Shape Algorithms)* 38(1):227–248, 2004.

25. A. Verroust and F. Lazarus. Extracting skeletal curves from 3D scattered data. In *The Visual Computer*, Springer, pp. 15–25, 2000.

26. Y. Lee, H. S. Kim and Lee S. Mesh parameterization with a virtual boundary. *Computers and Graphics* 26(5):677–686, 2002.

27. S. Haker, S. Angenent, A. Tannenbaum, R. Kikinis, G. Sapiro and M. Halle. Conformal surface parameterization for texture mapping. *IEEE Transactions on Visualization and Computer Graphics*, 6(2):181–189, 2000.

28. U. Pinkall and K. Polthier. Computing discrete minimal surfaces and their conjugates. *Experimental Mathematics*, 15–36, 1993.

29. M. Desbrun, M. Meyer and P. Alliez. Intrinsic parameterizations of surface meshes. In *Computer Graphics Forum*, vol. 21, pp. 209–218, 2001.

30. A. Sheffer and E. de Sturler. Parameterization of faceted surfaces for meshing using angle based flattening. *Engineering with Computers*, 17(3):326–337, 2000.

31. K. Hormann and G. Greiner. MIPS: An efficient global parametrization method. In *Curve and Surface Design: Saint-Malo*, Vanderbilt University Press, pp. 153–162, 1999.

32. M. Mortara, G. Patané, M. Spagnuolo, B. Falcidieno and J. Rossignac. Plumber: A multiscale decomposition of 3D shapes into tubular primitives and bodies. In *ACM Symposium on Solid Modelling*, pp. 339–344, 2004.

33. A. Fomenko and T. Kunii. *Topological Modeling for Visualization*. Springer, 1997.

34. D. Cohen-Steiner and J.-M. Morvan. Restricted delaunay triangulations and normal cycle. In *Proceedings of the Nineteenth Annual Symposium on Computational Geometry*, ACM Press, pp. 312–321, 2003.

35. M. Eck, T. DeRose, T. Duchamp, H. Hoppe, M. Lounsbery and W. Stuetzle. Multiresolution analysis of arbitrary meshes. In *Proceedings of the 22nd Annual Conference on Computer Graphics and Interactive Techniques*, ACM Press, pp. 173–182, 1995.

36. K. Hormann, U. Labsik and G. Greiner. Remeshing triangulated surfaces with optimal parameterizations. *Computer-Aided Design* 33(11):779–788, 2001.

37. V. Surazhsky and C. Gotsman. Explicit surface remeshing. In *Proceedings of the Eurographics/ACM SIGGRAPH Symposium on Geometry Processing*, Eurographics Association, pp. 20–30, 2003.

38. I. Guskov, K. Vidime, W. Sweldens and P. Schroeder. Normal meshes. In *Proceedings of the 27th Annual Conference on Computer Graphics and Interactive Techniques*, ACM Press/Addison-Wesley Publishing Co., pp. 95–102, 2000.

39. P. Alliez, M. Meyer and M. Desbrun. Interactive geometry remeshing. *Acm Transactions on Graphics*, 21(3):347–354, 2002.

40. H. Hoppe. Progressive meshes. In *Proceedings of the 23rd Annual Conference on Computer Graphics and Interactive Techniques*, ACM Press, pp. 99–108, 1996.

41. P. V. Sander, Z. J. Wood, S. J. Gortler, J. Snyder and H. Hoppe. Multi-chart geometry images. In *Proceedings of the Eurographics/ACM SIGGRAPH symposium on Geometry processing*, Eurographics Association, pp. 146–155, 2003.

42. P. V. Sander, J. Snyder, S. J. Gortler and H. Hoppe. Texture mapping progressive meshes. In *Proceedings of the 28th Annual Conference on Computer Graphics and Interactive Techniques*, ACM Press, pp. 409–416, 2001.

© The Eurographics Association and Blackwell Publishing Ltd 2004